Analysis and Prediction of Sulfate Erosion Damage of Concrete in Service Tunnel based on ARIMA Model

Dunwen Liu (dunwen@csu.edu.cn)
central south university
Haofei Chen
central south university
Yu Tang
central south university
Gong Chun
central south university
Yinghua Jian
central south university
Kunpeng Cao
central south university

Research Article

Keywords: Sulfate erosion, autoregressive integrated moving average (ARIMA), Elastic relative dynamic modulus(Erd)

Posted Date: July 24th, 2021

DOI: https://doi.org/10.21203/rs.3.rs-731283/v1

Analysis and prediction of sulfate erosion damage of concrete in service tunnel based on ARIMA model

Dunwen Liu[1], Haofei Chen[1], Yu Tang[1,*] , Gong Chun[1], Yinghua Jian[1], Kunpeng Cao[1]

[1]school of resources and safety engineering, central south university, Changsha, 410000, China.

*Correspondence should be addressed to Y.T.(email: tangyu9433@163.com)

ABSTRACT

Sulfate erosion is a major cause of concrete durability deteriorations, especially for the service tunnels which are in sulfate erosion for a long time. Accurately predicting the concrete damage failure under sulfate erosion has been a challenging problem in the evaluation and maintenance of concrete structures. Here we design the dry-wet cycle test of service tunnel concrete under sulfate erosion, and analyze the Elastic relative dynamic modulus（Erd） and mass under 35 times cycle periods. Then we develop an autoregressive integrated moving average (ARIMA) prediction model linking damage failure to Erd and mass. The results show that the deterioration of concrete first increased and then decreased with an extension of the dry–wet cycle period. Moreover, based on a finite set of training data, the proposed prediction approach shows high accuracy for the changes of concrete damage failure parameters in or out of the training dataset. The ARIMA method is proven to be feasible and efficient for predicting the concrete damage failure of service tunnel under sulfate erosion for a long time.

Introduction

With the popularization of concrete material, people began to use concrete material for infrastructure construction on a large scale. Concrete has also become the second most utilized building material after water[1]. Because concrete is widely used in a variety of environments, complex environmental factors will lead to premature failure and instability of concrete structures, among which sulfate erosion is the most critical factor to control the durability of concrete structures [2]. There are a large number of sulfate erosion strata in western China, and these corrosive substances may have corrosive effects on the tunnel lining in service [3]. Ma. first reported a case of damage to a concrete structure caused by the form of thiobacite during a 2004 survey of the Babanxia Hydropower Station in western China[4].In the Chengdu-Kunming Railway which has been built, a large number of erosion damage was found in the tunnel, which was analyzed as sulfate erosion damage. The physical crystallization and chemical erosion of sulfate are the main reasons for the spalling and loss of cement strength of the concrete lining of railway tunnels in Southwest China [5]. Prediction of erosion failure of the second lining concrete in service tunnel under sulfate erosion environment has become one of the problems to be solved urgently in tunnel construction.

The deterioration of concrete structure caused by sulfate erosion is manifested as the reaction of aggressive ions through hydration products in concrete and the formation of expansive materials. The most common minerals produced inside sulfate eroded tunnel concrete are gypsum and ettringite [6]. The evolution of tunnel concrete sulfate damage is often affected by sulfate concentration [7,8], temperature [9-11], humidity [12], concrete cement composition [13-15] and fly ash content [16,17] in the tunnel. Due to the complex damage mechanism

of concrete under sulfate erosion and numerous influencing factors, many scholars explored the damage failure mechanism of sulfate erosion through various experimental methods, so as to establish the research method of damage failure prediction of concrete under sulfate erosion. Rui He studied the damage mechanism of concrete at the microscopic level, namely the interfacial transition zone, under sulfate erosion in the process of dry-wet cycle. The results showed that with the increase of dry-wet cycle, the porosity of the interfacial transition zone gradually increased, and sulfate solution could compensate the microstructure of concrete [18]. Ren proposed a formula for calculating the reaction rate constant of gypsum based on the kinetics theory of chemical reaction, calculated the macroscopic tensile stress based on the volume fraction of gypsum, predicted the cycle times that concrete could bear, and then calculated the failure time of concrete [19]. Liao based on different soaking time of concrete under sulfate ion concentration distribution and nominal stress-strain curve, adopt the method of innovation for the different content of sulfate ion the true stress-strain curve of concrete, this paper proposes a concrete member structure can well predict sulfate erosion performance of actual constitutive model [20]. Silva immersed self-compacting concrete in 5% Na_2SO_4 and $MgSO_4$ solutions to evaluate the change in mass, loss of mechanical strength and linear expansion, which were reflected in the change in concrete length, loss of mass and compressive strength[21].

Although many scholars have focused on concrete sulfate erosion and explored it through experimental methods, the prediction of concrete damage failure for in-service tunnels is limited. ARIMA model was a time series prediction method proposed by Box Jenkins in 1976 that could be applied to small samples [22]. The ARIMA model is an extension of the ARMA model, including the autoregressive (AR) model, the moving average (MA) model and the Integrated method (I). ARIMA model is characterized by strong robustness, strong predictability of short time series and ease of application, and is widely used in the prediction of various disciplines [23]. K.E. Arunkumar used the ARIMA model and the SARIMA model to predict the prevalence trend of the COVID-19 pandemic in the top 16 countries with 70-80% of cumulative cases globally, revealing the future trend of COVID-19 outbreaks in the top 16 countries in 2019 [24]. Li used the ARIMA model and the LSTM model to predict the concentration of TSP in open-pit coal mines. Finally, several error statistical measures were used to evaluate the accuracy of the model, and sensitivity analysis was performed [25]. Wang combined the proposed non-linear metabolic gray model (NMGM) with the ARIMA model to create the NMGM-ARIMA technology, which can help researchers, policymakers, analysts and other stakeholders make more timely and accurate predictions of U.S. shale oil production[26].

In this paper, according to the essence of corrosion, the Erd and mass of concrete are taken as the basic indexes of damage and failure of concrete specimens [27,28]. Service tunnel concrete under the dual action of long-term sulfate erosion and dry-wet cycle was used to prepare specimens. Ultrasonic nondestructive testing method has been widely used in concrete nondestructive testing[29-32], using ultrasonic method to measure the damage degree of concrete. Through the correlation between the propagation velocity of ultrasonic pulse in concrete and the degree of damage inside concrete, the Erd of concrete is calculated by using the tested propagation velocity to reflect the degree of damage inside concrete. A three-dimensional hierarchical analysis method was used to process the relevant data and obtain the improved Erd after optimization. The subsequent damage failure time of the service tunnel

concrete prepared specimens was predicted by using the ARIMA model after optimization of the experimental data. The prediction results can provide some reference for the damage development and damage degree of concrete in tunnel.

Methods

Test principle

The change of the Erd of concrete can reflect the deterioration and compactness of the internal structure. When there are holes and cracks in the concrete, the ultrasonic wave will bypass the defects, resulting in the increase of sound propagation. When the concrete is eroded by sulfate, the porosity and compactness inside the concrete specimen are changed, which causes the change of ultrasonic speed. Therefore, the measurement of the ultrasonic speed of concrete specimens can effectively reflect the internal changes of concrete.

The acoustic parameter oscilloscope adopts an transmitting transducer to continuously transmit ultrasonic waves to the concrete. The ultrasonic waves propagate continuously between the concrete, and the receiving transducer at the other end receives the acoustic signals sent. The received signal is reflected on the oscilloscope by electronic technology, and the received electrical signal is amplified and quantified to obtain the acoustic parameters such as waveform, acoustic wave speed, amplitude, frequency and propagation time.

Test scheme

• *Test materials*

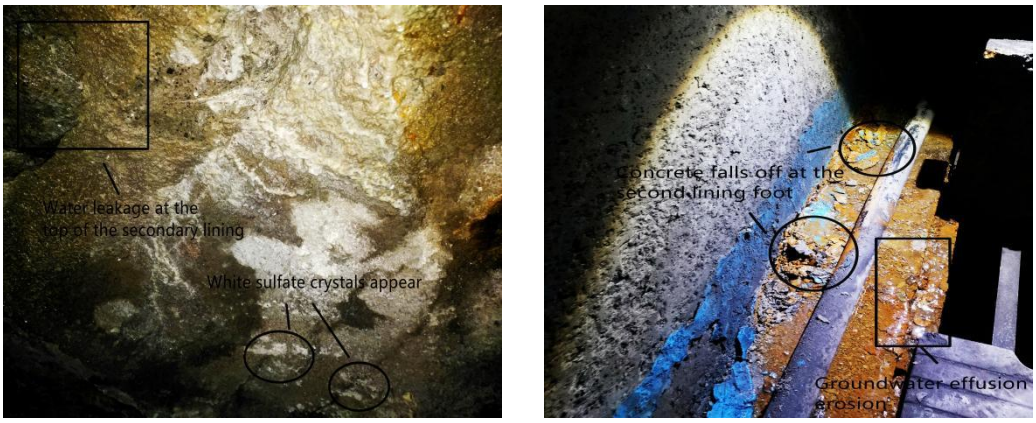

（a） （b）

Figure 1. Corrosion of tunnel :(a) sulfate crystals precipitated from tunnel concrete; (b) collapse and spalling of concrete with secondary lining feet

This research is based on a service highway tunnel in Chongqing, China. The highway tunnel was fully opened in 2006 and has a design life of 300 years. But in 2015 and 2018, there were a lot of disasters. As shown in Fig.1., the current situation of expansion and cracking of the secondary lining in the tunnel had been extended to the side wall of the secondary lining.

Table 1

Mixed proportion of concrete design in service of tunnel

Test Case Name	W/C	Water consumption （kg·m^3）	Gelled material （kg·m^3）	Aggregate （kg·m^3）	28 days compressive strength （MPa）

The ratio of the design	0.53	205	388	1813	39.5

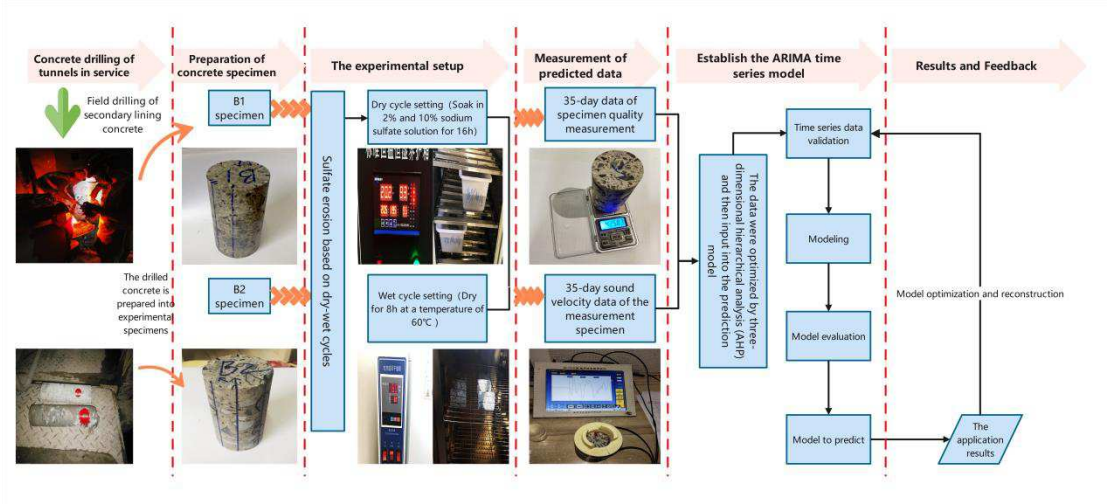

Figure 2. Schematic diagram of experiment and prediction process

In Fig.2, with the accumulation of time and long-term infiltration of groundwater, a large number of white sulfate crystals were produced on the secondary lining surface of the tunnel. The secondary lining concrete aggregate consists of machine-made sand with particle size of 0mm-4.75mm and continuous graded gravel with particle size of 5mm-25 mm. Polycarboxylate high efficiency water reducing agent (SP) was used as the admixture. The concrete strength and design mix ratio were shown in Table 1. In the tunnel sulfate corrosion of the secondary lining part of the core, made into a 50mm*100mm cylindrical test block. After curing and standing in the mold at a temperature of 20℃±5℃ for 24 h, the mold was then numbered and removed. After the mold was removed, it was immediately put into the standard curing room for maintenance. The temperature was set at 20℃±2℃, and the humidity RH was 95%.

• *Experimental environment*

We used dry-wet cycle experiment to accelerate sulfate erosion. The degradation mechanism of concrete blocks in the accelerated experiment is consistent with that of concrete in service[18], so it is necessary to select the appropriate concentration of sulfate solution.

Table 2

Tunnel water sample testing

Term	Ca^{2+}	Mg^{2+}	Na^{+}	SO_4^{2-}	Cl^{-}	HCO_3^{-}
ZK83+551	309.56	61.21	17.65	761.69	1.17	102.31
ZK83+509	317.15	66.53	15.54	699.33	1.18	116.90
ZK83+565	448.00	71.80	18.97	1020.04	1.20	122.77
ZK83+535	451.81	70.23	18.75	815.14	0.18	122.77
ZK83+523	419.86	68.68	16.44	824.05	1.18	116.92

The concentration of sulfate suggested by Chinese standard GB/T 50,082 is 5% for the evaluation of concrete. However, due to the high sulfate concentration in the water sample detection of the test tunnel (See Table.2) and the experiment requires a strict sulfate concentration. According to the standard of environmental action classification in the 《Code for Durability

Design of Concrete Structures》 (GB/T 50476-2008), the sulfate concentration of the water sample was more than 200mg/L, and the corrosion is Grade D (severe). Therefore, sodium sulfate immersion concentrations of 2% and 10% are selected, which are also used in previous studies [33,34]. To ensure the concentration of the sodium sulfate soaking solution remains unchanged, replace it every 30 times. The soaking box used in the experiment is the constant temperature concrete curing box YH-40B, and the drying box is the electric heating air blowing drying box DHG 101-2B.

Test procedure

Fig. 2. shows the test and prediction process scheme diagram. The test procedure is as follows:

(1) The prepared concrete specimens are numbered B1 and B2, and then put into the designed sulfate solution. The specimens are accelerated sulfate corrosion by dry-wet cycles. The cycle period is 24h, of which 16h is the soaking period. We put it into the soaking box with 2% and 10% sodium sulfate solution to ensure that the concrete specimens are fully soaked. The temperature is set at 20℃, and the relative humidity is 95%. After soaking for 16h, the concrete specimens are taken out and put into the electric air drying box for drying, and the drying temperature is set at 60℃.

(2) Taking the specimens out and placing it in a ventilated place to cool to room temperature. The four directions and axial directions of the side of the concrete test block are taken for ultrasonic nondestructive testing. The first wave method is used to measure the longitudinal ultrasonic speed of concrete specimen during the ultrasonic nondestructive testing. To ensure the accuracy of experimental data and reduce the systematic errors generated in the instrument, experimental environment and first-wave pickup, the plexiglass test block with the same size as the specime is used as the calibration test block during the test in this experiment. When analyzing the change of ultrasonic speed of the specimen, the difference between the actual ultrasonic speed measured by the specimen and the ultrasonic speed measured by the calibration test block on the same date is used as the analysis object.

$$\Delta v = v_{the\ experimental\ specimen} - v_{organic\ glass} \quad (1)$$

The acoustic coupling phenomenon will affect the transmission of ultrasonic wave in the detected object and affect the detection result. Therefore, a coupling agent (honey was used in this paper) is used on the inspection surface to enhance the penetration ability of ultrasonic wave.

(3) Repeat steps (1) and (2) for a cycle after the single measurement.

Data analysis method

• *Calculation of integrated wave velocity*

As the corrosion aging process inside the concrete is not uniform, so there is a difference in the corrosion degree in each direction. In this test, acoustic velocity in five directions was obtained for each test. The three-dimensional analytic hierarchy process (AHP) was used to analyze the acoustic velocity in different directions to obtain the comprehensive acoustic velocity. The calculation formula is as follows:

$$V_0' = \sqrt{\left(\omega_1 V_1'\right)^2 + \left(\omega_2 V_2'\right)^2 + \left(\omega_3 V_3'\right)^2 + \left(\omega_4 V_4'\right)^2 + \left(\omega_5 V_5'\right)^2} \quad (2)$$

Where， $V_1^{'}$、$V_2^{'}$、$V_3^{'}$、$V_4^{'}$ and $V_5^{'}$ are longitudinal wave velocities in five directions，m/s；

$V_0^{'}$ is the comprehensive initial longitudinal wave velocity，m/s； w_1、w_2、w_3、w_4 and w_5 are the weights of longitudinal wave velocity in each direction.

• *Elastic relative dynamic modulus*

Chinese standard GB/T50082-2009 stipulates that when the Erd is reduced to 60%, it is judged as the failure of concrete specimen. Because there is liquid in the concrete, the ultrasonic test error will be affected, so the test time is set to two hours after the natural heat dissipation after drying. According to Equations (3) and (4), it can be calculated.

$$E_d = \frac{(1+\mu)(1-2\mu)}{(1-\mu)}\rho V^2 \quad (3)$$

$$E_{rd} = \frac{E_t}{E_0} = \frac{V_t^2}{V_0^2} \quad (4)$$

Where μ is Poisson's ratio; ρ is the density of concrete (kg/m^3); V is the speed of sound during ultrasonic test; V_0 and V_t are respectively the acoustic velocity of the concrete specimen without the dry-wet cycles and the acoustic velocity of the concrete specimen after the dry-wet cycles.

• *Mass data*

An electronic scale with an inductivity of 0.01g was used to test the mass loss of concrete after each dry-wet cycle. Referring to the experimental method (21) in GB/T50082-2009, when the mass loss of concrete reaches 5%, the concrete is judged to have failed. Calculation formula for mass loss of concrete specimen.

Prediction method

• *ARIMA model*

ARIMA model is a model established by using difference method to obtain stationary data from non-stationary data in ARMA model.It includes AR model, MA model and Difference (I) method.ARIMA has three characteristics: p, d, q, where p is the order of the AR term, q is the order of the MA term, and d is the difference order required to make the time series stable.

The difference method eliminates the changes on the level of time series, and it is necessary to difference the unstable data for the prediction of the ARIMA model. To ensure the effective use of data, the model can extract useful information by second-order difference at most. Among them, the first-order difference and second-order difference can be expressed mathematically by the equation

First difference: $y_t' = y_t - y_{t-1}$ (5)

Second difference: $y_t'' = y_t - 2y_{t-1} + y_{t-2}$ (6)

$$AR: \quad y_t = c + \alpha_1 y_{t-1} + \alpha_2 y_{t-2} + \Lambda + \alpha_p y_{t-p} + \varepsilon_t$$

（7）

$$MA:\ y_t = c + \varepsilon_t + \theta_1\varepsilon_{t-1} + \theta_2\varepsilon_{t-2} + \ldots\ldots + \theta_p\varepsilon_{t-p}$$

（8）

$$ARIMA:\ y_t = c + \alpha_1 y_{t-1} + \alpha_2 y_{t-2} + \Lambda + \alpha_p y_{t-p} + \varepsilon_t + \theta_1\varepsilon_{t-1} + \theta_2\varepsilon_{t-2} + \Lambda + \theta_q\varepsilon_{t-q}$$

（9）

Where y_t is the non-stationary time series data, is the observed value of the time stamp. y_{t-i} is the past time series value, y_{t-2} is the observed value of the time stamp, y_t' is the time series after the first-order difference of the non-stationary time series, y_t'' is the time series after the second-order difference.c is the intercept constant term, α_i is the autoregressive average model coefficient, θ_i is the moving average model coefficient, and ε_t is the white noise process with the variance of σ^2 .

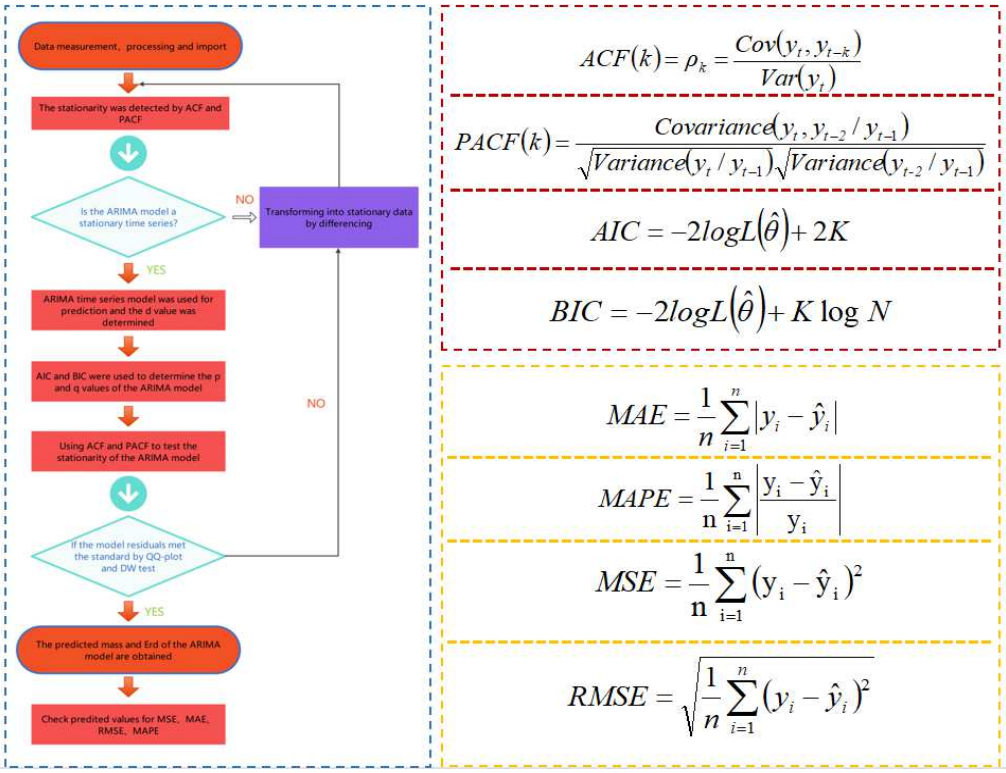

Figure.3. Algorithm showing the methodology for developing ARIMA models

Fig. 3. shows the calculation frame diagram of the ARIMA model established by MATLAB, which can obtain a fairly stable time series prediction model of ARIMA mass and Erd according to the specific calculation framework.The lag k refers to the correlation between the observed data with an interval of k time periods. In the expression of PACF function, k=2 is taken. $log\ L(\hat{\theta})$ is the likelihood function, K is the total number of model parameters, N is the number of observations. $\hat{y}_i$ is model predicted value, y_i is actual value.The established regression model was evaluated according to MAE, MSE and RMSE.

• *Test of model data： ACF and PACF*

The test of data stability is an important step in time series analysis.The autocorrelation function (ACF) and partial autocorrelation function (PACF) of autocorrelation graph are used to test the data stability. ACF is the correlation between the former time series data and the present time series data. It describes the linear relationship between the observed values at the moment t and the moment (t-k).PACF eliminated the influence of other random variables.It simply measured the correlation between time series data and lag value.

• *Fitting model data： AIC and BIC*

The minimum criterion method of Akagi Information Criterion (AIC) and Bayesian Information Criterion (BIC) was used to determine the order p and q of the model. AIC based on the concept of entropy, is a standard to measure the optimal fitness of statistical models. It encourages the optimal fitness of data fitting but tries to avoid overfitting. BIC is a basic method in statistical pattern recognition. Bayesian decision criterion not only considers the probability of the occurrence of various reference populations, but also considers the loss caused by misjudgment.Both AIC and BIC used the penalty likelihood criterion.Compared with AIC and BIC, BIC imposes a greater penalty on the model.Thus BIC will obtain a more simplified model. In the AIC and BIC Settings, a lower value represents the best model and has a higher likelihood value.

• *Residual test of the model*:QQ-plot and DW test

ARIMA model needs to carry out residual test to ensure that the order is appropriate.。The residual test includes QQ-plot (quantile-quantile plot) test and Dubin-Watson test. QQ-plot test is used to intuitively verify whether a set of data is normally distributed. If the sample data deviates too much from the line, the unreasonable model will be shown.Dubin-Watson test is the test statistic of residual autocorrelation of diagnostic model proposed by Dubin and Waston.

• *Error estimation*

The prediction accuracy is evaluated by the mean absolute error (MAE), mean absolute percentage error (MAPE), mean square error (MSE) and root mean square error (RMSE).

Results

Mass change

The mass was measured 35 times in the experiment, with the first 30 times for analysis and the last 5 times for predictive testing.

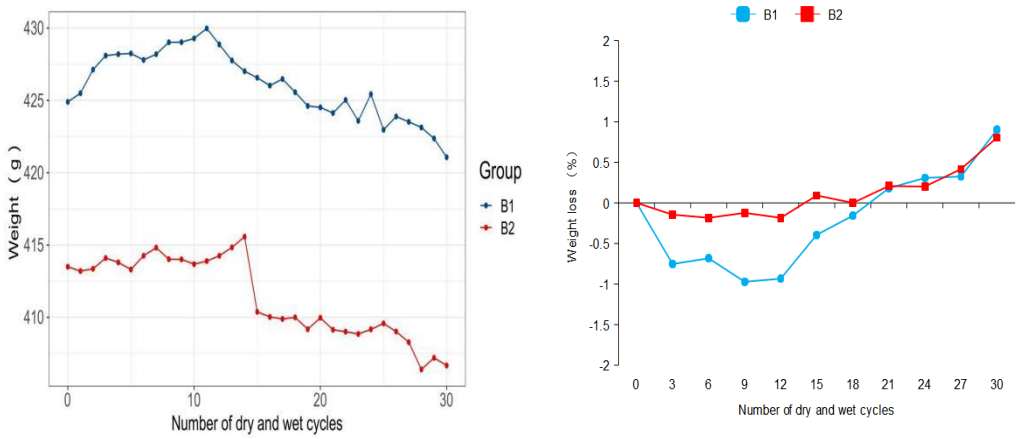

Figure.4. Mass changes of concrete specimens

In Fig.4., the mass of B1 and B2 shows a trend of slow rise, then a trend of rapid decline after leveling off. After dry-wet cycles for 30 times, the mass loss rates of B1 and B2 were 0.901 and 0.805, respectively.This is due to the sulfate ions into the concrete after the reaction with the internal hydration products, resulting in erosion products in the pore accumulation, thus filling the pores. In a certain period of time, the further reaction of sulfate solution is blocked. The compactness of concrete is temporarily improved, so the mass is increased to a certain extent. However, after several dry-wet cycle, crystalline salt will be generated at the outer pore of concrete specimen.The erosion products generated inside have expansionability, so the crystalline salt expansion stress will be generated, resulting in cracking and spallation of concrete, and the mass will be greatly reduced. The solution concentration of B2 was low and sulfate ions enter the concrete less, so the mass loss before 12 times was less. In the later stage of erosion, the mass loss of concrete didn't increase significantly due to the generation of erosion products and the shedding of aggregate.The mass of B2 decreased significantly after the 15th dry-wetting cycle because of the shedding of coarse aggregate.

Elastic relative Dynamic Modulus

The combined ultrasonic speed of 35 dry-wet cycles tests were obtained and the Erd were calculated.

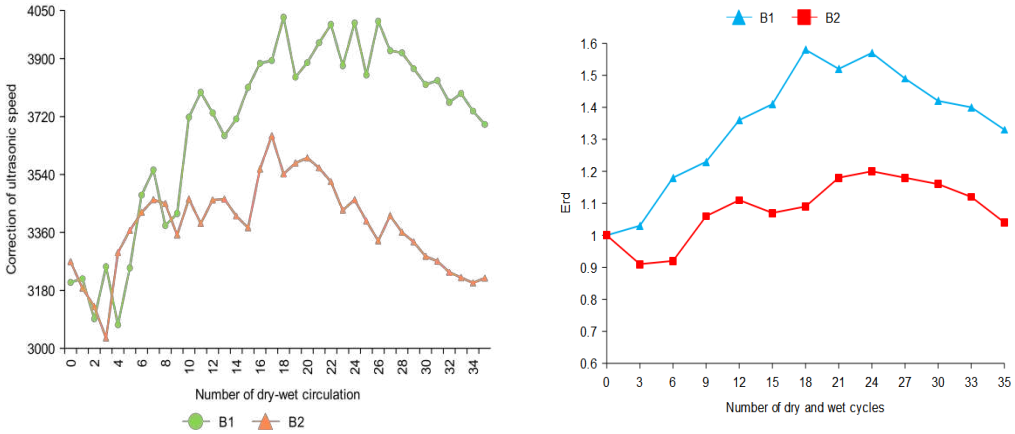

Figure.5. Changes in ultrasonic speed of concrete specimens after the correction of three-dimensional tomographic analysis

In Fig.5. , the change of ultrasonic speed of B2 was relatively gentle compared with that of B1. Because B2 is immersed in 2%Na2SO4 solution. The corrosion of B2 was relatively slow, and the internal expansion product accumulation rate was also slow. When the specimen B1 was immersed in 10%Na2SO4, the change of ultrasonic speed was the most obvious.

As the different sulfate concentrations, the amount of sulfate ions in the solution entered the concrete in the same time was different. The Erd of specimen B2 decreased in the first three cycle of drying and wetting. This was because the concentration of B2 erosion solution was low, and the generation rate of internal expansion products was less than the damage of specimen in the soaking and drying cycles. So the Erd decreased accordingly. With the increase of the number of dry-wet cycles, the internal expansion product accumulated. The accumulated amount was greater than the damage amount of soaking drying cycles. After the descending stage, B1 and B2 showed an obvious upward trend due to the continuous accumulation of expansion products. After the 24th dry-wet cycle, the expansion products were generated in large quantities to produce

expansive force, and the internal compactness of concrete decreases. A large number of expansion products will also produce micro-cracks in the specimens, which will promote the degradation of concrete, resulting in the decline of Erd of B1 and B2.

Prediction based on ARIMA time series

• *Stationary analysis of time series data*

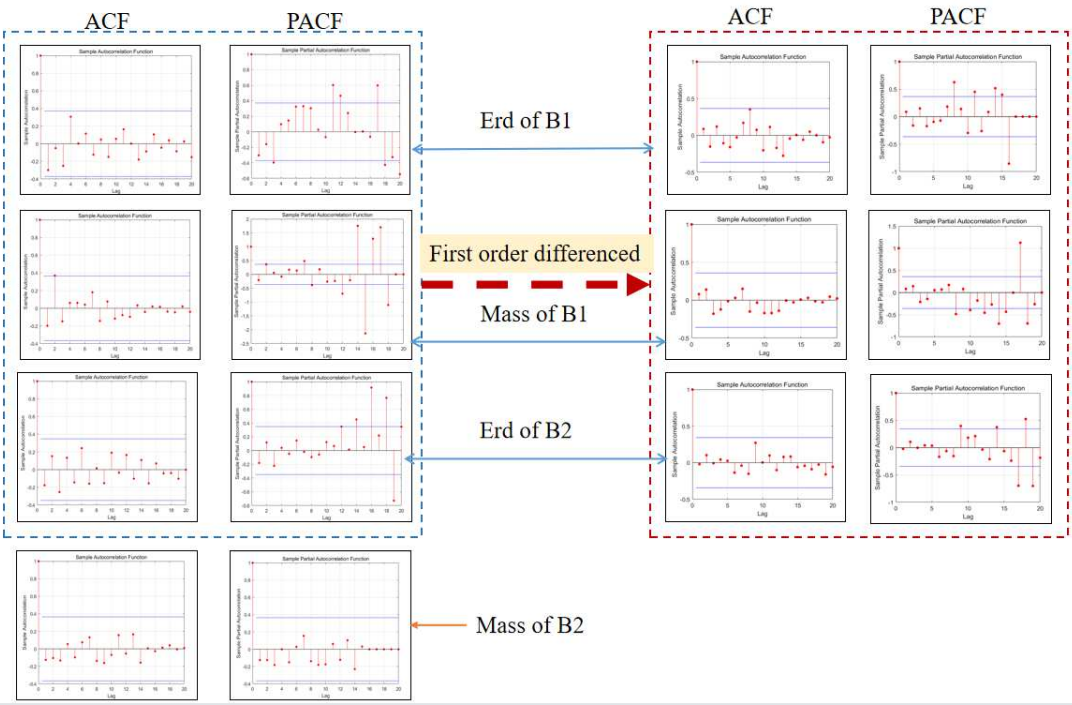

Figure.6. The initial data stability of B1 and B2 was tested by ACF and PACF test and post-difference test

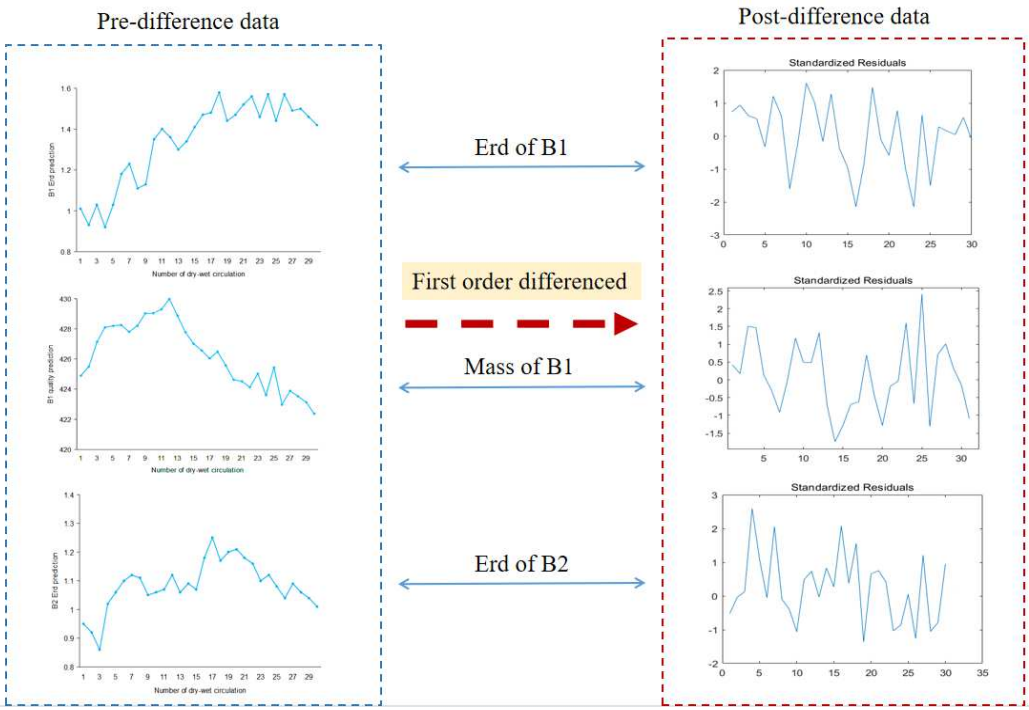

Figure. 7. First-order difference of ARIMA model

Fig.6. shows ACF, PACF test and post-difference test for the initial data stability of B1 and B2. Before the first difference， it showed that the trailing of PACF graph didn't tend to 0 and the sharp value is too large. It was judged that the mass and Erd of B1 and the Erd of B2 belong to non-stationary time series data. So it was necessary to make difference to them to maintain the stationarity of the time series of ARIMA model. Then, p and q values of B1 and B2 ARIMA models were obtained by AIC and BIC ordering methods.

Fig.7. shows the first-order difference graphs of ARIMA (2,1,1), ARIMA (5,1,3) and ARIMA (3,1,3). It can be seen that after first-order difference, the trend of the original sequence (the trend must be non-stationary) is eliminated. The whole sequence basically oscillates around the determined mean value. Compared with the first-order difference, the second-order difference only enlarges the amplitude of the oscillation, so it is more appropriate to adopt the first-order difference for this sequence. In general, the first - order and second - order difference can make the sequence become stable.

Table 3

ARIMA model was selected to predict the damage and failure of sulfate erosion specimens

Specimen to predict	ARIMA（p、d、q）	MSE	MAE	RMSE	MAPE	DW	Loss of failure
B1 Mass Prediction	（2,1,1）	0.06809	0.236	0.2609	0.00281	1.7824	59 times (403.3)
Prediction of of B1 Erd	（5,1,3）	0.00084	0.028	0.0290	0.1019	1.8081	53 times (0.535)
B2 Mass Prediction	（1,0,1）	0.19636	0.4	0.4431	0.00467	2.2272	103 times (392.65)
Prediction of of B2 Erd	（3,1,3）	0.0003	0.014	0.01732	0.0721	1.9091	101 times (0.596)

In order to ensure that the order of the ARIMA model was consistent, ACF and PACF graphs were used to test the stationarity of the model again. After the difference of the model, it can be seen that the ACF autocorrelation functions tend to 0 in the end.The number of sharp red sites in the PACF figure is greatly reduced and the value is also decreasing.It proves that the model has become a stationary time series after the difference, and effective data has been input into the model.

By comparing the mass prediction and the Erd prediction, it can be found that the final trailing of the mass prediction tends to be 0. The Erd still tends to be slow after the difference. According to the stationary analysis, the mass prediction is selected as the better model for damage failure prediction.

• *Residual test of ARIMA model*

In order to check whether the ARIMA model conforms to the application of prediction, the residual test is carried out.

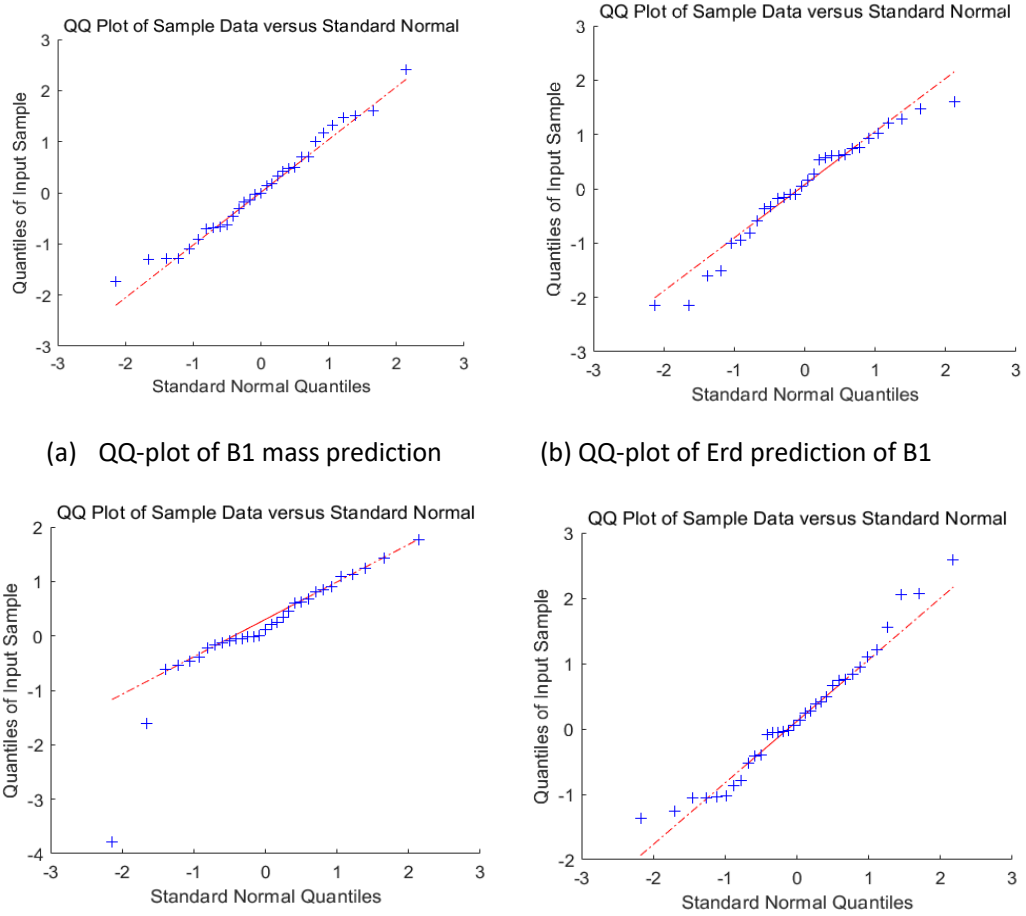

(a) QQ-plot of B1 mass prediction (b) QQ-plot of Erd prediction of B1

（c）QQ-plot of B2 mass prediction （d）QQ-plot of Erd prediction of B2

Figure. 8. Erd of B1 and B2 and residual test of mass prediction model QQ-Plot

In Fig. 8., the linear graph of residual followed a linear relationship with the quantile, and all the sites were distributed near the line. Although the observed P value of the late sites didn't significantly exceed the expected value, they were close to the expected value. So the analysis model was reasonable. DW test shows that the DW value of the two models is close to 2, so this model doesn't belong to the autocorrelation model.

When selecting mass prediction and relative motion prediction, it can be seen that the lower left corner of QQ-plot of mass prediction is the sites with low significance, that is, the sites that are not associated with traits are determined. The observed P value of these sites should be consistent with the expected value. In the upper right corner of the graph are the sites with high significance, which are potential candidate sites associated with traits. These points are located above the diagonal, that is, the observed P value of the site exceeds the expected value. This indicates that the effect of these sites exceeds the random effect, which in turn indicates that these sites are significantly correlated with the traits. This also means that the mass prediction represents a better model choice.

• *Prediction model evaluation*

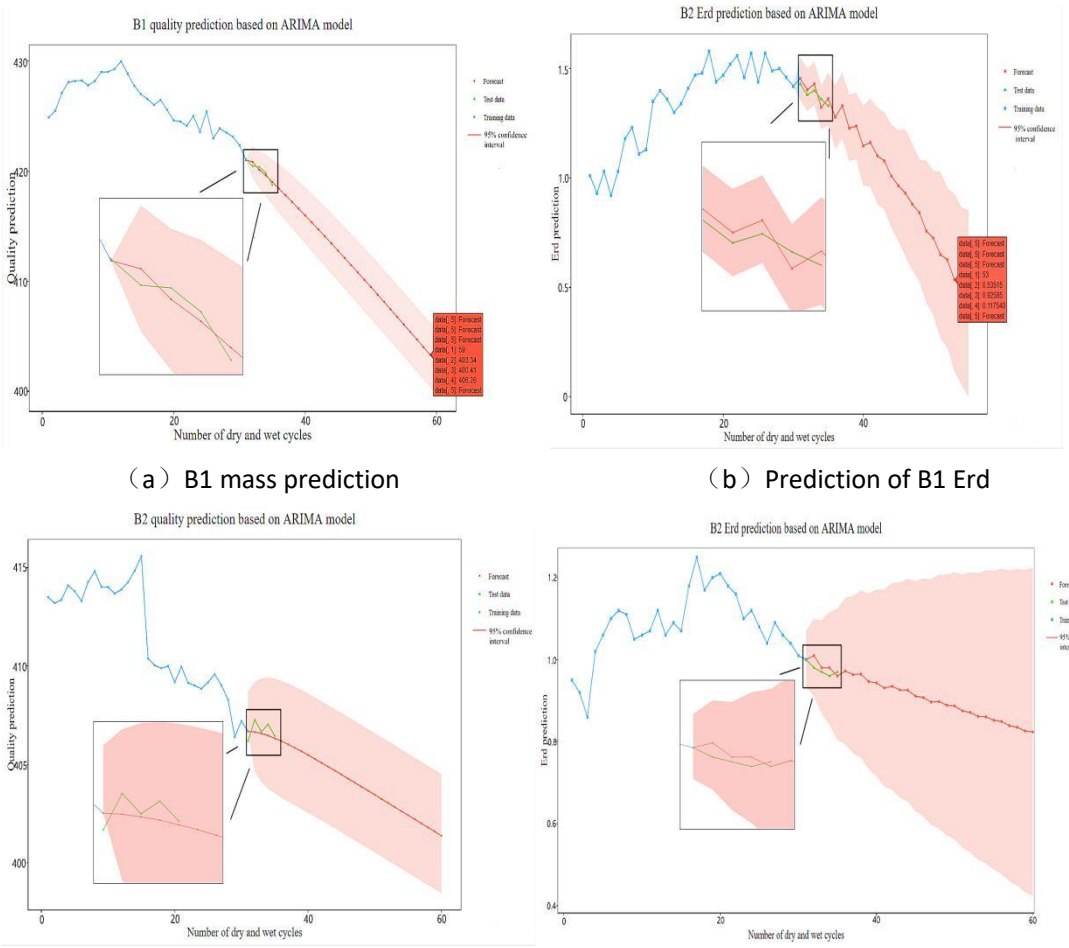

（a）B1 mass prediction　　（b）Prediction of B1 Erd

（c）B2 mass prediction　　（d）Prediction of B2 Erd

Figure. 9. ARIMA time series model prediction of mass and Erd of B1 and B2

Fig. 9. (a) and (c) show the mass prediction of B1 and B2 under the dry-wet cycle. Fig. 9 (b) and (d) show the Erd prediction of B1 and B2 under the dry-wet cycles. In Fig.9., the blue line represents the experimental training data, the green line represents the actual measurement data, and the red line represents the forecast trend data. The red line area represents the 95% confidence interval of the forecast data. According to Fig.9. and Table 3., since B1 and B2 adopt first-order difference, the values of p and q are all less than 2, then the ARIMA model is a low-order model. It shows that the mass prediction model has an obvious trend of change.So the fluctuation of B1 in mass prediction is small, and finally it is transformed into a quasi-linear line. When the Erd prediction model adopts the first-order difference, the values of p and q are 5, and then the ARIMA model is a high-order model. This indicates that the change trend of Erd is not obvious and there is obvious oscillation. Therefore, according to the previous experimental training data, the forecast curve is oscillating at the beginning and then smoothing out at the end.

Through the exercise of the previous experimental training data, the prediction curves of B1 and B2 were compared. It can be found that both the mass prediction and the Erd prediction of B1 within 30 times, the Erd loss value of the specimen is 60% (mass loss is 5%). At this point, the sulfate attacks the concrete to the point of damage and failure. However, the prediction curve of B2 is slow, and the failure times of sulfate erosion loss are about 70 times. This is due to the different sulfate concentrations of B1 and B2, the erosion rate of B1 is obviously greater than that of B2, and the predicted failure times of B2 are also greater than that of B1.

According to the prediction results, the mass loss of B1 is predicted to reach 5% after the 59th dry-wet cycle to reach damage failure, and the mass is only 403.3g. The Erd of elasticity decreased to less than 60% after the 53rd dry-wet cycle and reached loss failure, with a time span of 6 times. The mass prediction of B2 stops after the 103rd dry-wet cycle, and the mass loss reaches 5% to reach the loss failure. The Erd stops after the 101rd dry-wet cycle and drops below 60% to reach the loss failure. The time span is 2 times. Therefore, it can be mutually verified that the optimization effect of the model is good, and the prediction results are accurate.The difference of damage failure time between the two methods is not big.

Based on the mass of ARIMA time series and the accuracy of the Erd prediction model were compared. The results of mass prediction and Erd prediction were given in table 4.

Table 4

ARIMA time series prediction table

(a) Predicted value and error analysis of time series B1

Dry-wet cycle	B1 mass measurement value	ARIMA mass prediction value	B1 Erd measurement value	Predicted value of Erd of ARIMA
31	421.07	421.03	1.43	1.45
32	420.46	420.84	1.38	1.40
33	420.4	420.14	1.40	1.43
34	419.85	419.63	1.36	1.32
35	418.74	419.02	1.33	1.36
B1 mass prediction:	MAE=0.236	MSE=0.06808	RMSE=0.2609	MAPE=0.00281
B1 Erd prediction:	MAE=0.028	MSE=0.00084	RMSE=0.0290	MAPE=0.1019

(b) Predicted value and error analysis of time series B2

Dry-wet cycle	B2 mass measurement value	ARIMA mass prediction value	B2 Erd measurement value	Predicted value of Erd of ARIMA
31	406.18	406.68	1.00	1.00
32	407.27	406.65	0.98	1.01
33	406.66	406.57	0.97	0.98
34	407.04	406.47	0.96	0.98
35	406.45	406.33	0.97	0.96
B2 mass prediction:	MAE=0.4	MSE=0.19636	RMSE=0.4431	MAPE=0.00467
B2 Erd prediction:	MAE=0.014	MSE=0.0003	RMSE=0.0173	MAPE=0.0721

According to Table 3 and 4, both the MSE, MAE, RMSE and MAPE of the mass loss prediction and the Erd prediction are relatively small.It indicates that the deviation between the experimental measured value and the predicted value of the ARIMA model is small. The optimization and prediction effect of the ARIMA model is good. By comparing the mass loss prediction with the Erd loss prediction, it can be found that the MSE, MAE and RMSE values of the mass loss prediction are all small. But the MAPE value is obviously larger than the value of the Erd loss. This is because the mass value itself is large and the fluctuation range is large, so the above situation occurs. For QQ-Plot, ACF and PACF plots, it can also be judged that the mass loss prediction of sulfate erosion failure stability and optimization degree based on ARIMA model are better than the Erd. In conclusion, the prediction accuracy and results of mass loss prediction of sulfate erosion failure based on the ARIMA time series model are better than those based on the Erd of ARIMA time series.

The reason is that in the case of a small number of samples, the variation trend of mass loss prediction is simple and presents less volatility. The variation trend of Erd loss prediction is complex and has high volatility, which requires the development of a large number of optimized control parameters and a relatively large training database.

Discussion

In this study, the concrete secondary lining of tunnel in service was used to prepare specimens. The internal corrosion condition was retained to carry out the dry-wet cycles sulfate erosion accelerated test. Through several dry-wet cycles experiments and ultrasonic nondestructive testing methods, the mass loss and the influence of relative motion model on the service tunnel concrete which has been eroded by sulfate for a long time are discussed.The following conclusions can be drawn:

(1) With the increase of dry-wetting cycles, the mass loss rate of the specimen showed a trend of decreasing slowly and then increasing rapidly after leveling off. The Erd decreases in the early stage due to the damage of soaking drying cycle, and increases rapidly in the later stage, then decreases slowly after leveling off.

(2) Apply the ARIMA prediction model to the prediction of sulfate erosion of concrete in tunnels in service. The time and development trend of concrete sulfate erosion failure were obtained by mass prediction and Erd prediction. Through the ARIMA model stability, residual test, MSE, MAE, RMSE and MAPE and other judgment basis. A better mass loss prediction model was selected to predict the sulfate erosion specimen. It has the characteristics of higher precision and better prediction effect.

(3) According to the experiment and prediction, the sulfate erosion degree of the tunnel in service can be obtained. It has reference significance to judge the timely protection of the secondary lining of the tunnel in service and whether it needs to be dismantled. It can greatly improve the safety and utilization degree of the tunnel in service and reduce the economic loss.

References:

1. Monteiro, P., S.A. Miller and A. Horvath, Towards sustainable concrete. *Nat Mater,* 2017. **16**(7): p. 698-699.doi: 10.1038/nmat4930.
2. Hartell, J.A., A.J. Boyd and C.C.Ferraro, Sulfate Attack on Concrete: Effect of Partial Immer sion. *Journal of Materials in Civil Engineering*, 2011(No.5): p. 572-579,doi:10.1061/(ASCE)MT.19 43-5533.0000208
3. Lei, M., et al., Experimental study on the damage mechanism of tunnel structure suffering fr om sulfate attack. *Tunnelling and underground space technology*, 2013.**36**:p.5-13.https://doi.org/1 0.1016/j.tust.2013.01.007.
4. Ma, B., et al., Thaumasite formation in a tunnel of Bapanxia Dam in Western China. *Cement and Concrete Research*, 2006. **36**(4): p. 716-722.doi: https://doi.org/10.1016/j.cemconres.2005.10.011.
5. Huang Bo et al., Analysis of railway tunnel lining damage in southwest China. *Railway Construction*, 2010(05): 48-52.doi:CNKI:SUN:TDJZ.0.2010-05-017.
6. González, M.A. and E.F. Irassar, ETTRINGITE FORMATION IN LOW C3A PORTLAND CEMENT EXPOSED TO SODIUM SULFATE SOLUTION. *Cement and concrete research*, 1997. **27**(7): p. 1061-1071.doi: https://doi.org/10.1016/j.cemconres.2005.10.011
7. Hossack, A.M.A.H. and M.D.A.M. Thomas, The effect of temperature on the rate of sulfate attack of Portland cement blended mortars in Na2SO4 solution. *Cement & Concrete Research*, 2015: p. 136-

142.doi:10.1016/j.cemconres.2015.02.024.
8. Zanqun, L., et al., Physicochemical Study on the Interface Zone of Concrete Exposed to Different Sulfate Solutions. *Journal of Wuhan University of Technology*. Materials science edition, 2006. **21**(z1): p. 167-174.doi:CNKI:SUN:WLGY.0.2006-S1-037.
9. Santhanam, M., M.D. Cohen and J. Olek, Modeling the effects of solution temperature and concentration during sulfate attack on cement mortars. *Cement and concrete research*, 2002. **32**(4): p. 585-592.doi: 10.1016/S0008-8846(01)00727-X.
10. Al-Dulaijan, S.U., Sulfate resistance of plain and blended cements exposed to magnesium sul fate solutions. *Construction & building materials,* 2007. **21**(8): p. 1792-1802.doi: 10.1016/j.conbuil dmat.2006.05.017.
11. Jiang, X., et al., Effect of temperature on durability of cement-based material to physical sulf ate attack. *Construction & building materials,* 2021. **266**: p. 120936.doi: 10.1016/j.conbuildmat.20 20.120936.
12. Liu, Z., et al., Micro-analysis of the role of interfacial transition zone in "salt weathering" on concrete. *Construction & building materials*, 2010. **24**(11): p. 2052-2059.doi: 10.1016/j.conbuildm at.2010.04.053.
13. Kang Jingfu, Several Basic Problems in the Study of Concrete Sulfate Erosion. *Concrete*, 1995(03): pp. 9-18.doi:CNKI:SUN:HLTF.0.1995-03-001.
14. Liu, S., et al., High-Durability Concrete with Supplementary Cementitious Admixtures Used in Corrosive Environments. *Crystals (Basel)*, 2021. **11**(2): p. 196.doi: 10.3390/cryst11020196.
15. Liu, P., et al., Effect of physical and chemical sulfate attack on performance degradation of c oncrete under different conditions. *Chemical physics letters*, 2020. **745**: p. 137254.doi: 10.1016/j.c plett.2020.137254.
16. Dzunuzovic, N., et al., External sulfate attack on alkali-activated fly ash-blast furnace slag co mposite. *Construction & building materials*, 2017. **157**: p. 737-747.doi: 10.1016/j.conbuildmat.201 7.09.159.
17. Cheng, S., et al., Effects of fly ash, blast furnace slag and metakaolin on mechanical properties and durability of coral sand concrete. *Applied clay science*, 2017. **141**: p. 111-117. doi: 10.1016/j.clay.2017.02.026.
18. He, R., et al., Damage mechanism and interfacial transition zone characteristics of concrete under sulfate erosion and Dry-Wet cycles. *Construction & building materials,* 2020. **255**(C): p. 119340.doi: 10.1016/j.conbuildmat.2020.119340.
19. Ren, J., et al., The damage mechanism and failure prediction of concrete under wetting–drying cycles with sodium sulfate solution. *Construction & building materials*, 2020. **264**: p. 120525.doi: 10.1016/j.conbuildmat.2020.120525.
20. Liao, K., et al., Modeling constitutive relationship of sulfate-attacked concrete. *Construction & building materials*, 2020. **260**: p. 119902.doi: 10.1016/j.conbuildmat.2020.119902.
21. Silva, Y.F. and S. Delvasto, Sulfate attack resistance of self-compacting concrete with residue of masonry. *Construction & building materials*, 2021. **268**.doi: 10.1016/j.conbuildmat.2020.121095.
22. G.E. Box, G.M. Jenkins, Time Series Analysis: Forecasting and Control,revised ed., San Francisco, 1976.
23. Jafarian Namin, S., et al., Annual forecasting of inflation rate in Iran: Autoregressive integrated moving average modeling approach. *Engineering reports (Hoboken, N.J.)*, 2021. **3**(4): p. n/a-n/a.doi: 10.1002/eng2.12344.

24. ArunKumar, K.E., et al., Forecasting the dynamics of cumulative COVID-19 cases (confirmed, recovered and deaths) for top-16 countries using statistical machine learning models: Auto-Regressive Integrated Moving Average (ARIMA) and Seasonal Auto-Regressive Integrated Moving Average (SARIMA). *Applied soft computing*, 2021. **103**: p. 107161.doi: 10.1016/j.asoc.2021.107161.
25. Li, L., et al., Monitoring and prediction of dust concentration in an open-pit mine using a deep-learning algorithm. *Journal of environmental health science and engineering*, 2021. **19**(1): p. 401-414.doi: 10.1007/s40201-021-00613-0.
26. Wang, Q., Song, X., Li, R..A novel hybridization of nonlinear grey model and linear ARIMA residual correction for forecasting U.S. shale oil production[J].*Energy*,2018,**165**,1320-1331. doi:10.1016/j.energy.2018.10.032.
27. Al-Hamrani, A., et al., Green Concrete for a Circular Economy: A Review on Sustainability, Durability, and Structural Properties. *Materials*, 2021. **14**(2): p. 351.doi: 10.3390/ma14020351.
28. Algourdin, N., et al., Durability of recycled fine mortars under freeze – thaw cycles. *Construction and Building Materials*, 2021. **291**: p. 123330.doi: https://doi.org/10.1016/j.conbuildmat.2021.123330.
29. Cheng, H.X., et al., The Design Of The Ultrasonic Nondestructive Testing System Based On The EMAT. *MATEC web of conferences*, 2016. **44**: p. 2065.doi: 10.1051/matecconf/20164402065.
30. Lee, T. and J. Lee, Setting time and compressive strength prediction model of concrete by nondestructive ultrasonic pulse velocity testing at early age. *Construction & building materials*, 2020. **252**: p. 119027.doi: 10.1016/j.conbuildmat.2020.119027.
31. Rashidyan, S., T. Ng and A. Maji, Estimating the Depth of Concrete Pier Wall Bridge Foundations Using Nondestructive Sonic Echo. *Journal of nondestructive evaluation*, 2017. **36**(3): p. 1-17.doi: 10.1007/s10921-017-0433-5.
32. Solís-Carcaño, R. and E.I. Moreno, Evaluation of concrete made with crushed limestone aggregate based on ultrasonic pulse velocity. *Construction & building materials*, 2008. **22**(6): p. 1225-1231.doi: 10.1016/j.conbuildmat.2007.01.014
33. Zeidan, M., M.T. Bassuoni and A. Said, Physical salt attack on concrete incorporating nano-s ilica. *Journal of sustainable cement based materials*, 2017. **6**(3): p. 195-216.doi: 10.1080/2165037 3.2016.1218802.
34. Alyami, M.H., et al., Potential accelerated test methods for physical sulfate attack on concret e. *Construction and Building Materials*, 2019. **229**: p. 116920.doi: https://doi.org/10.1016/j.conbuil dmat.2019.116920.

Acknowledgements

The research has been supported by the Initiation fund for postdoctoral research of Central South University, grant number 228697.

Author Contributions

The experiments and ideas for this article were conceived by L.D.W.. J.Y.H.,C.K.P., C.H.F.and G.C.participated in the design, measurement and completion of the experiments. The experimental results were analyzed and discussed by C.H.F., G.C.and T.Y.. T.Y. and L.D.W. provided guidance and review for the whole paper. All authors have read and agreed to the published version of the manuscript.

Additional Information

Competing financial interests: The authors declare no competing financial interests.